Photosynthesis and Bioenergetics

Edited by

James Barber

Imperial College London, UK

Alexander V Ruban

Queen Mary University of London, UK

Published by

World Scientific Publishing Co. Pte. Ltd.

5 Toh Tuck Link, Singapore 596224

USA office: 27 Warren Street, Suite 401-402, Hackensack, NJ 07601 UK office: 57 Shelton Street, Covent Garden, London WC2H 9HE

British Library Cataloguing-in-Publication Data A catalogue record for this book is available from the British Library.

PHOTOSYNTHESIS AND BIOENERGETICS

Copyright © 2018 by World Scientific Publishing Co. Pte. Ltd.

All rights reserved. This book, or parts thereof, may not be reproduced in any form or by any means, electronic or mechanical, including photocopying, recording or any information storage and retrieval system now known or to be invented, without written permission from the publisher.

For photocopying of material in this volume, please pay a copying fee through the Copyright Clearance Center, Inc., 222 Rosewood Drive, Danvers, MA 01923, USA. In this case permission to photocopy is not required from the publisher.

ISBN 978-981-3230-29-3

Typeset by Stallion Press Email: enquire@stallionpress.com

Printed in Singapore

Preface

This book covers some of the most recent advances in the fields of Bioenergetics and Photosynthesis presented at an international workshop held in the Institute of Advanced Studies (IAS), Nanyang Technological University (NTU), Singapore, from 21st to 23rd March, 2016. The meeting was held as a tribute to Jan Anderson FRS who passed away in August 2015 and to celebrate the 75th birthdays of Leslie Dutton FRS and John Walker FRS, Nobel Laureate. Contributions to the workshop and to this book, are from outstanding scientists which includes the Nobel Laureate Rudolph Marcus (Chapter 2 by Marcus and Volkán-Kacsó) who created a theory of electron transport reactions. Marcus first provided the kinetic and thermodynamic description of the movement of electrons between molecules — a chemical processes at the very heart of the biological electron transfer in the major classes of bioenergetic systems such as bacterial cells, mitochondria and chloroplasts. Not surprisingly, the theme of electron transport reactions in the key redox enzymatic complexes of mitochondria and chloroplasts is covered in the majority of chapters of this book. Indeed, Chapters 3 (Wikström) and 4 (Rich) are dedicated to cytochrome c oxidase — a complex that terminates the respiratory electron transport chain producing water as a by-product. The most recent advances in studies of cytochrome c oxidase, photosystem II (PSII), that splits water and produces oxygen, are thoroughly reviewed in Chapters 5 (Kaucikas et al.) and 6 (Barber). The recent structural advances in understanding photosystem I that functions in series with PSII, are covered in Chapter 7 (Nelson). In modern times the science of bioenergetics attained an extraordinary progress with development and applications of state-of-the-art techniques, such as femtosecond crystallography (Chapter 5, Kaucikas et al.); single molecule microscopy and spectroscopy,

(Chapter 2, Marcus and Volkán-Kacsó); combination of electron and confocal fluorescence microscopy (Chapter 9, Ruban; Chapter 10, Koochak *et al.*). A significant pool of chapters is dedicated to the regulatory processes that take place in the photosynthetic electron transport chain owing to the dynamic nature of the photosynthetic membrane organisation reviewed in Chapter 10 by Koochak *et al.* These mechanisms include regulation of the photosynthetic light harvesting (Chapter 9, Ruban), cyclic electron transport (Chapter 12, Kou *et al.*; Chapter 13, Hanke and Schreibe and Chapter 14, Larkum *et al.*) and the whole oxygenic electron transport chain (Chapter 11, Järvi *et al.*). Chapter 8 by Shivhare and Mueler-Cajar, summarises the recent progress in understanding the protein *rubisco activase* that regulates the most abundant enzyme, Rubisco (ribulose-1,5-bisphosphatecarboxylase/oxygenase) in the biosphere and is responsible for carbon fixation. And finally, the ideas and the most recent developments in the field of applications of the knowledge of Bioenergetics and Photosynthesis are discussed in Chapter 1 (Ennist *et al.*) and Chapter 6 (Barber).

We recommend this book to specialists in Bioenergetics and Photosynthesis, researchers and postgraduate students who are working and studying various aspects of respiratory and photosynthetic electron transport chains as well as dynamic regulation of the light harvesting and electron transport events in oxygenic photosynthesis.

We would like to acknowledge IAS and NTU for supporting and hosting the workshop in March 2015 and encouraging us to produce this book.

J. Barber and A. V. Ruban London, 7 June 2017

Contents

Foreword b Preface	y James Barber FRS	v vii
Chapter 1	Redox-active Proteins	1
Martin J. l	Ennist, Joshua A. Mancini, Dirk B. Auman, Chris Bialas, wanicki, Tatiana V. Esipova, Bohdana M. Discher, er C. Moser and P. Leslie Dutton	
		2
1. Introdu		2 3 3
	te protein strategy cognizing natural complexity	3
2.1. Ke	Helical scaffolds common in natural protein structures reveal	
∠,∠, α +ħ.	e basics of how cofactors are ligated and positioned	5
0.2 E	rst-principles of de novo designed protein structures outlined	ϵ
2.3. II	ectron transfer in protein understood for engineering	12
2.4. Lit	al Strategies for Development of Functional Light- and	
	active Proteins	14
2 1 T a	essons learned from the first heme protein maquettes	14
3.1. 1.0	paracterization of one maquette promotes development of others	16
3,2, C	2.1 Charge-activated conformational switch in a homodimeric	
5.	four-α-helix heme B protein [Grosset et al., 2001]	16
3	2.2. Electron tunneling between monolayers of	
J.	linked-homodimeric heme protein and gold electrodes	
	[Chen et al., 1999; 2002]	17
	L	

and a state of the	
3.2.3. Linked-homodimeric heme protein oxygen transporter	19
[Koder et al., 2009]	20
4. Single-chain Four-α-Helix Maquettes	
4.1. From disulfide linked homodimeric bundles to single-chain	20
four-α-helix structures	
4.2. Compatibility of single-chain four- α -helix maquettes	22
with natural proteins	
4.2.1. Single-chain four-α-helix heme B maquette interactions	22
with natural cytochrome c	22
4.2.2. In vivo single-chain four-o-helix protein covalently	24
linking heme C: a novel cytochrome c	25
5. Prospects and Previews	27
Acknowledgements	27
References	Las
Chapter 2 Free, Stalled, and Controlled Rotation Single Molecule	
Experiments on F ₁ -ATPase and their Relationships	35
Sándor Volkán-Kacsó and Rudolph A. Marcus	
1. Introduction	35
Description of Three Single-Molecule Experiments	37
2.1. Free rotation experiments: Stepping rotation	
and concerted kinetics	37
2.2. Stalling experiments	38
2.3. Controlled rotation experiments	40
3. Group Transfer Theory in Stalling and Controlled	•
Rotation Experiments	40
3.1. Angle dependent rate constants and free energies	41
3.1. Angle dependent rate constants and θ -range 3.2. Application to ATP binding in the overlapping θ -range	43
3.3. Turnover, near symmetry and long binding events	
in the controlled rotation experiments	44
4. Application of the Theory to Free Rotation	46
4.1. Rate constant of a free rotation experiment	46
4.1. Relation between controlled and free rotation experiments	47
4.3. Use of the rate constant <i>versus</i> rotor angle data	
to predict the step size and dwell angles in free rotation	49
	50
5. Concluding Remarks	50
Acknowledgements	50
Appendix Evaluation of Eq. (8):	50
Evaluation of Eq. (8) References	51

Contents	хi
----------	----

Chapter 3 The Role of the H-Channel in Cytochron A Commentary	me c Oxidase: 55
Mårten Wikström	55
1. Introduction	55 56
2. Conservation of the H-Channel Structure	30
3. The Linkage of Proton Pumping to Individual Steps	57
of the Catalytic Cycle	59
4. The Proton Pump Cycle	60
5. Conclusions	61
Acknowledgements References	61
	- tions from
Chapter 4 Cytochrome c Oxidase: Insight into Fu	logue 65
Studies of the Yeast S. cerevisiae Homo	logue
Peter R. Rich	<i>(</i>
1. Introduction: Catalysis, Coupling and Efficiency	65 CO Superfamily 67
a Competency and Functional Variations in the fit	Oupoix
3. Yeast CcO — A Link Between Mammalian and Al	Bacterial Cos 70
3.1. The H channel and its possible roles	71
3.2. Supernumerary and additional subunits	74
4. Concluding Remarks	75
Acknowledgements References	75
Chapter 5 Femtosecond Infrared Crystallograph Photosystem II Core Complexes: Water Exciton Dynamics and Charge Separa Real Space and Time	ching
Marius Kaucikas, James Barber, Thomas Renger and Jasper J. van Thor	
	82
Introduction Femtosecond Infrared Crystallography	83
2. Grammany of Theory for Exciton Dynamics	ographic Case 85
and Transing by Electron Transfer for the Crystallographic Case	
4 Earth accord Infrared Crystallography of Exciton Dynamics	
5 Structural Measurement of the Charge Separated S	State 1 680 /1 1100
5.1 Vibrational mode assignments of the P_{680}/P_{680}	105
Pheo-/Pheo spectra 5.2 Fitting the P_{680}^{+}/P_{680} and Pheo-/Pheo FTIR spec	ectra 109

	5.3 Fitting the 832 ps TR-IR crystallography spectra	109
6.	Implications for Light Harvesting Function of	110
_	PSII Core Complexes	114
Re	eferences	
CI	hapter 6 Bioenergetics, Water Splitting and	118
	Artificial Photosynthesis	117
Ja	mes Barber	
1	Introduction	118
	Photosystem II (PSII)	120
L.	2.1. The catalytic centre	121
	2.2. Synthetic cubane mimics	125
3	Mechanism of Water Splitting	126
٦.	3.1. Base-catalysed nucleophilic attack mechanism	126
	3.2. Indirect support for the nucleophilic mechanism	
	for O-O bond formation in PSII	128
	3.3. Comparison with Fe-Ni carbon monoxide dehydrogenase	
	(CODH)	129
	3.4. Ligands to the Mn ₄ Ca ²⁺ O ₅ cluster	131
4.	Synthesized Chemical Model Systems	132
•••	4.1. Mechanism of O ₂ production from organo-Ru	
	complexes	132
	4.2. Mechanism of O ₂ production from organo-Mn complexes	134
5.	Alternative Mechanisms are Less Compelling	135
	Artificial Photosynthesis	136
	Conclusions	138
	eferences	140
~	hapter 7 A Quest for the Atomic Resolution of	
U	Chapter 7 A Quest for the Atomic Resolution of Plant Photosystem I	149
N	Tathan Nelson	
		149
	. Introduction . The Structure of Plant PSI	150
	. The Structure of Plant PSI . The Light Harvesting Complex of Plant PSI	154
		155
	acknowledgements	155
- 15	Leferences	

Chapter 8 Rubisco Activase: The Molecular Chiropractor of the World's Most Abundant Protein Devendra Shivhare and Oliver Mueller-Cajar 1. Introduction 2. The Most Abundant Protein on Earth is a Poor Catalyst 2.1. The structure and diversity of Rubisco 2.2. Reaction mechanism: co-factor binding and catalysis 2.3. Rubisco is prone to inhibition by sugar phosphates 3.1. Rubisco Activase, the Molecular Chiropractor 3.1. Rubisco activases are members of the AAA+ family of proteins 3.2. Oligomeric state and mechanism of the Rubisco activase 3.3. Regulation of Rubisco activase 3.4. The role of Rubisco activase in regulating photosynthesis at elevated temperatures 4. Outlook References Chapter 9 Adaptive Reorganisation of the Light Harvesting Anteuna Alexander V. Ruban 1. Introduction 2. The Structure of LHCII Complex and the Landscapes of the Photosystems 3. Evidence for the Fast Dynamics of the Photosynthetic Membrane 4. LHCII Composition and Membrane Dynamics 5. State Transitions are Affected by PSII Antenna Composition 6. Zeaxanthin and Non-Photochemical Quenching Modulate LHCII Dynamics 6. 1. LHCII clustering versus mobility 6. 2. NPQ control by LHCII antenna hydrophobicity 7. Formation of the NPQ Quencher(s): Inner LHCII Complex Dynamics 8. Physiological Implications of the Dynamic Properties of LHCII Acknowledgements 212	Contents	xiii
1. Introduction 159 2. The Most Abundant Protein on Earth is a Poor Catalyst 160 2.1. The structure and diversity of Rubisco 161 2.2. Reaction mechanism: co-factor binding and catalysis 163 2.3. Rubisco is prone to inhibition by sugar phosphates 164 3. Rubisco Activase, the Molecular Chiropractor 167 3.1. Rubisco activases are members of the AAA+ family of proteins 168 3.2. Oligomeric state and mechanism of the Rubisco activase 171 3.3. Regulation of Rubisco activase 172 3.4. The role of Rubisco activase in regulating photosynthesis at elevated temperatures 174 4. Outlook 175 4. Outlook 177 Chapter 9 Adaptive Reorganisation of the Light Harvesting Antenna 189 Alexander V. Ruban 190 2. The Structure of LHCII Complex and the Landscapes of the Photosystems 191 3. Evidence for the Fast Dynamics of the Photosynthetic Membrane 195 4. LHCII Composition and Membrane Dynamics 197 5. State Transitions are Affected by PSII Antenna Composition 198 6. Zeaxanthin and Non-Photochemical Quenching Modulate LHCII Dynamics 6.1. LHCII clustering versus mobility 201 6.2. NPQ control by LHCII antenna hydrophobicity 203 7. Formation of the NPQ Quencher(s): Inner LHCII Complex Dynamics 207 8. Physiological Implications of the Dynamic Properties of LHCII Acknowledgements 212	Chapter 8 Rubisco Activase: The Molecular Chiropractor of the World's Most Abundant Protein	159
1. Introduction 159 2. The Most Abundant Protein on Earth is a Poor Catalyst 160 2.1. The structure and diversity of Rubisco 161 2.2. Reaction mechanism: co-factor binding and catalysis 163 2.3. Rubisco is prone to inhibition by sugar phosphates 164 3. Rubisco Activase, the Molecular Chiropractor 167 3.1. Rubisco activases are members of the AAA+ family of proteins 168 3.2. Oligomeric state and mechanism of the Rubisco activase 171 3.3. Regulation of Rubisco activase 172 3.4. The role of Rubisco activase in regulating photosynthesis at elevated temperatures 174 4. Outlook 175 4. Outlook 177 Chapter 9 Adaptive Reorganisation of the Light Harvesting Antenna 189 Alexander V. Ruban 190 2. The Structure of LHCII Complex and the Landscapes of the Photosystems 191 3. Evidence for the Fast Dynamics of the Photosynthetic Membrane 195 4. LHCII Composition and Membrane Dynamics 197 5. State Transitions are Affected by PSII Antenna Composition 198 6. Zeaxanthin and Non-Photochemical Quenching Modulate LHCII Dynamics 6.1. LHCII clustering versus mobility 201 6.2. NPQ control by LHCII antenna hydrophobicity 203 7. Formation of the NPQ Quencher(s): Inner LHCII Complex Dynamics 207 8. Physiological Implications of the Dynamic Properties of LHCII Acknowledgements 212	Devendra Shivhare and Oliver Mueller-Cajar	
2. The Most Abundant Protein on Earth is a Poor Catalyst 2.1. The structure and diversity of Rubisco 2.2. Reaction mechanism: co-factor binding and catalysis 2.3. Rubisco is prone to inhibition by sugar phosphates 3. Rubisco Activase, the Molecular Chiropractor 3.1. Rubisco activases are members of the AAA+ family of proteins 3.2. Oligomeric state and mechanism of the Rubisco activase 3.3. Regulation of Rubisco activase 3.4. The role of Rubisco activase in regulating photosynthesis at elevated temperatures 4. Outlook References Chapter 9 Adaptive Reorganisation of the Light Harvesting Antenna Alexander V Ruban 1. Introduction 2. The Structure of LHCII Complex and the Landscapes of the Photosystems 3. Evidence for the Fast Dynamics of the Photosynthetic Membrane 4. LHCII Composition and Membrane Dynamics 5. State Transitions are Affected by PSII Antenna Composition 6. Zeaxanthin and Non-Photochemical Quenching Modulate LHCII Dynamics 6.1. LHCII clustering versus mobility 6.2. NPQ control by LHCII antenna hydrophobicity 7. Formation of the NPQ Quencher(s): Inner LHCII Complex Dynamics 8. Physiological Implications of the Dynamic Properties of LHCII Acknowledgements 2.12	1 Introduction	159
2.1. The structure and diversity of Rubisco 2.2. Reaction mechanism: co-factor binding and catalysis 2.3. Rubisco is prone to inhibition by sugar phosphates 3. Rubisco Activase, the Molecular Chiropractor 3.1. Rubisco activases are members of the AAA+ family of proteins 3.2. Oligomeric state and mechanism of the Rubisco activase 3.3. Regulation of Rubisco activase 3.4. The role of Rubisco activase in regulating photosynthesis at elevated temperatures 4. Outlook References Chapter 9 Adaptive Reorganisation of the Light Harvesting Antenna Alexander V. Ruban 1. Introduction 2. The Structure of LHCII Complex and the Landscapes of the Photosystems 3. Evidence for the Fast Dynamics of the Photosynthetic Membrane 4. LHCII Composition and Membrane Dynamics 5. State Transitions are Affected by PSII Antenna Composition 6. Zeaxanthin and Non-Photochemical Quenching Modulate LHCII Dynamics 6.1. LHCII clustering versus mobility 6.2. NPQ control by LHCII antenna hydrophobicity 7. Formation of the NPQ Quencher(s): Inner LHCII Complex Dynamics 8. Physiological Implications of the Dynamic Properties of LHCII Acknowledgements 163 164 165 166 167 168 167 168 167 168 168 167 168 168 169 169 168 169 169 168 169 168 169 169 168 169 169 169 169 169 169 169 169 169 169	2. The Most Abundant Protein on Earth is a Poor Catalyst	160
2.2. Reaction mechanism: co-factor binding and catalysis 2.3. Rubisco is prone to inhibition by sugar phosphates 164 3. Rubisco Activase, the Molecular Chiropractor 3.1. Rubisco activases are members of the AAA+ family of proteins 168 3.2. Oligomeric state and mechanism of the Rubisco activase 3.3. Regulation of Rubisco activase 3.4. The role of Rubisco activase in regulating photosynthesis at elevated temperatures 4. Outlook References Chapter 9 Adaptive Reorganisation of the Light Harvesting Antenna 1. Introduction 2. The Structure of LHCII Complex and the Landscapes of the Photosystems 3. Evidence for the Fast Dynamics of the Photosynthetic Membrane 4. LHCII Composition and Membrane Dynamics 5. State Transitions are Affected by PSII Antenna Composition 6. Zeaxanthin and Non-Photochemical Quenching Modulate LHCII Dynamics 6.1. LHCII clustering versus mobility 6.2. NPQ control by LHCII antenna hydrophobicity 7. Formation of the NPQ Quencher(s): Inner LHCII Complex Dynamics of LHCII Acknowledgements 168 167 168 168 169 168 169 168 169 168 169 168 169 168 169 169 168 171 168 172 172 173 174 175 175 177 177 177 177 177 178 179 179 189 190 190 190 191 191 192 193 194 195 196 197 197 198 199 199 199 199 190 190 190 190 190 190	2.1 The structure and diversity of Rubisco	161
2.3. Rubisco is prone to inhibition by sugar phosphates Rubisco Activase, the Molecular Chiropractor 3.1. Rubisco activases are members of the AAA+ family of proteins 3.2. Oligomeric state and mechanism of the Rubisco activase 3.3. Regulation of Rubisco activase 3.4. The role of Rubisco activase in regulating photosynthesis at elevated temperatures 4. Outlook References Chapter 9 Adaptive Reorganisation of the Light Harvesting Antenna Introduction 190 The Structure of LHCII Complex and the Landscapes of the Photosystems Evidence for the Fast Dynamics of the Photosynthetic Membrane HHCII Composition and Membrane Dynamics Evidence for the Fast Dynamics of the Photosynthetic Membrane LHCII Composition and Membrane Dynamics Evacuanthin and Non-Photochemical Quenching Modulate LHCII Dynamics LHCII clustering versus mobility Evacuation of the NPQ Quencher(s): Inner LHCII Complex Dynamics Physiological Implications of the Dynamic Properties of LHCII Acknowledgements	2.2 Reaction mechanism: co-factor binding and catalysis	
3. Rubisco Activase, the Molecular Chiropractor 3.1. Rubisco activases are members of the AAA+ family of proteins 3.2. Oligomeric state and mechanism of the Rubisco activase 3.3. Regulation of Rubisco activase 3.4. The role of Rubisco activase in regulating photosynthesis at elevated temperatures 4. Outlook References Chapter 9 Adaptive Reorganisation of the Light Harvesting Antenna 1. Introduction 2. The Structure of LHCII Complex and the Landscapes of the Photosystems 3. Evidence for the Fast Dynamics of the Photosynthetic Membrane 4. LHCII Composition and Membrane Dynamics 5. State Transitions are Affected by PSII Antenna Composition 6. Zeaxanthin and Non-Photochemical Quenching Modulate LHCII Dynamics 6.1. LHCII clustering versus mobility 6.2. NPQ control by LHCII antenna hydrophobicity 7. Formation of the NPQ Quencher(s): Inner LHCII Complex Dynamics 6. Physiological Implications of the Dynamic Properties of LHCII Acknowledgements 168 168 168 171 168 168 172 168 173 168 174 168 175 174 174 175 175 176 177 178 179 179 179 179 179 179 179 179 179 179	2.3 Rubisco is prone to inhibition by sugar phosphates	
3.1. Rubisco activases are members of the AAA+ family of proteins 3.2. Oligomeric state and mechanism of the Rubisco activase 3.3. Regulation of Rubisco activase 3.4. The role of Rubisco activase in regulating photosynthesis at elevated temperatures 4. Outlook References Chapter 9 Adaptive Reorganisation of the Light Harvesting Antenna 1. Introduction 2. The Structure of LHCII Complex and the Landscapes of the Photosystems 3. Evidence for the Fast Dynamics of the Photosynthetic Membrane 4. LHCII Composition and Membrane Dynamics 5. State Transitions are Affected by PSII Antenna Composition 6. Zeaxanthin and Non-Photochemical Quenching Modulate LHCII Dynamics 6.1. LHCII clustering versus mobility 6.2. NPQ control by LHCII antenna hydrophobicity 7. Formation of the NPQ Quencher(s): Inner LHCII Complex Dynamics 8. Physiological Implications of the Dynamic Properties of LHCII Acknowledgements 171 172 173 174 175 175 176 177 178 179 189 190 190 190 190 190 190 190 190 190 19	3 Rubisco Activase, the Molecular Chiropractor	167
of proteins 3.2. Oligomeric state and mechanism of the Rubisco activase 3.3. Regulation of Rubisco activase 3.4. The role of Rubisco activase in regulating photosynthesis at elevated temperatures 4. Outlook References Chapter 9 Adaptive Reorganisation of the Light Harvesting Antenna Alexander V. Ruban 1. Introduction 2. The Structure of LHCII Complex and the Landscapes of the Photosystems 3. Evidence for the Fast Dynamics of the Photosynthetic Membrane 4. LHCII Composition and Membrane Dynamics 5. State Transitions are Affected by PSII Antenna Composition 6. Zeaxanthin and Non-Photochemical Quenching Modulate LHCII Dynamics 6.1. LHCII clustering versus mobility 6.2. NPQ control by LHCII antenna hydrophobicity 7. Formation of the NPQ Quencher(s): Inner LHCII Complex Dynamics 6. Physiological Implications of the Dynamic Properties of LHCII Acknowledgements 171 172 173 174 175 175 177 189 199 190 190 190 191 191 192 193 194 195 197 197 198 199 197 198 198 199 199 199 199 199 199 199 199	3.1 Rubisco activases are members of the AAA+ family	•
3.2. Oligomeric state and mechanism of the Rubisco activase 3.3. Regulation of Rubisco activase 3.4. The role of Rubisco activase in regulating photosynthesis at elevated temperatures 4. Outlook References 177 Chapter 9 Adaptive Reorganisation of the Light Harvesting Antenna Alexander V. Ruban 1. Introduction 2. The Structure of LHCII Complex and the Landscapes of the Photosystems 3. Evidence for the Fast Dynamics of the Photosynthetic Membrane 4. LHCII Composition and Membrane Dynamics 5. State Transitions are Affected by PSII Antenna Composition 6. Zeaxanthin and Non-Photochemical Quenching Modulate LHCII Dynamics 6.1. LHCII clustering versus mobility 6.2. NPQ control by LHCII antenna hydrophobicity 7. Formation of the NPQ Quencher(s): Inner LHCII Complex Dynamics 8. Physiological Implications of the Dynamic Properties of LHCII Acknowledgements 2010 2012 2012 2016 2017 2017 2018 2019 2019 2019 2019 2019 2019 2019 2019		
3.3. Regulation of Rubisco activase 3.4. The role of Rubisco activase in regulating photosynthesis at elevated temperatures 4. Outlook References 175 Chapter 9 Adaptive Reorganisation of the Light Harvesting Antenna 189 Alexander V. Ruban 1. Introduction 2. The Structure of LHCII Complex and the Landscapes of the Photosystems 3. Evidence for the Fast Dynamics of the Photosynthetic Membrane 4. LHCII Composition and Membrane Dynamics 5. State Transitions are Affected by PSII Antenna Composition 6. Zeaxanthin and Non-Photochemical Quenching Modulate LHCII Dynamics 6.1. LHCII clustering versus mobility 6.2. NPQ control by LHCII antenna hydrophobicity 7. Formation of the NPQ Quencher(s): Inner LHCII Complex Dynamics 8. Physiological Implications of the Dynamic Properties of LHCII Acknowledgements 212	3.2. Oligomeric state and mechanism of the Rubisco activase	
3.4. The role of Rubisco activase in regulating photosynthesis at elevated temperatures 4. Outlook References 175 References 177 Chapter 9 Adaptive Reorganisation of the Light Harvesting Antenna 189 Alexander V. Ruban 1. Introduction 190 2. The Structure of LHCII Complex and the Landscapes of the Photosystems 191 3. Evidence for the Fast Dynamics of the Photosynthetic Membrane 195 4. LHCII Composition and Membrane Dynamics 197 5. State Transitions are Affected by PSII Antenna Composition 198 6. Zeaxanthin and Non-Photochemical Quenching Modulate LHCII Dynamics 200 6.1. LHCII clustering versus mobility 201 6.2. NPQ control by LHCII antenna hydrophobicity 203 7. Formation of the NPQ Quencher(s): Inner LHCII Complex Dynamics 207 8. Physiological Implications of the Dynamic Properties of LHCII Acknowledgements 212	3.3. Regulation of Rubisco activase	172
photosynthesis at elevated temperatures 4. Outlook References Chapter 9 Adaptive Reorganisation of the Light Harvesting Antenna Alexander V. Ruban 1. Introduction 190 2. The Structure of LHCII Complex and the Landscapes of the Photosystems 191 3. Evidence for the Fast Dynamics of the Photosynthetic Membrane 195 4. LHCII Composition and Membrane Dynamics 197 5. State Transitions are Affected by PSII Antenna Composition 6. Zeaxanthin and Non-Photochemical Quenching Modulate LHCII Dynamics 6.1. LHCII clustering versus mobility 6.2. NPQ control by LHCII antenna hydrophobicity 7. Formation of the NPQ Quencher(s): Inner LHCII Complex Dynamics 8. Physiological Implications of the Dynamic Properties of LHCII Acknowledgements 212	3.4. The role of Rubisco activase in regulating	
4. Outlook References Chapter 9 Adaptive Reorganisation of the Light Harvesting Antenna 189 Alexander V. Ruban 1. Introduction 2. The Structure of LHCII Complex and the Landscapes of the Photosystems 3. Evidence for the Fast Dynamics of the Photosynthetic Membrane 4. LHCII Composition and Membrane Dynamics 5. State Transitions are Affected by PSII Antenna Composition 6. Zeaxanthin and Non-Photochemical Quenching Modulate LHCII Dynamics 6.1. LHCII clustering versus mobility 6.2. NPQ control by LHCII antenna hydrophobicity 7. Formation of the NPQ Quencher(s): Inner LHCII Complex Dynamics 8. Physiological Implications of the Dynamic Properties of LHCII Acknowledgements 210 212	photosynthesis at elevated temperatures	
Chapter 9 Adaptive Reorganisation of the Light Harvesting Antenna 189 Alexander V. Ruban 1. Introduction 190 2. The Structure of LHCII Complex and the Landscapes of the Photosystems 191 3. Evidence for the Fast Dynamics of the Photosynthetic Membrane 195 4. LHCII Composition and Membrane Dynamics 197 5. State Transitions are Affected by PSII Antenna Composition 198 6. Zeaxanthin and Non-Photochemical Quenching Modulate LHCII Dynamics 200 6.1. LHCII clustering versus mobility 201 6.2. NPQ control by LHCII antenna hydrophobicity 203 7. Formation of the NPQ Quencher(s): Inner LHCII Complex Dynamics 207 8. Physiological Implications of the Dynamic Properties of LHCII 2112 Acknowledgements 2110		
Alexander V. Ruban 1. Introduction 2. The Structure of LHCII Complex and the Landscapes of the Photosystems 3. Evidence for the Fast Dynamics of the Photosynthetic Membrane 4. LHCII Composition and Membrane Dynamics 5. State Transitions are Affected by PSII Antenna Composition 6. Zeaxanthin and Non-Photochemical Quenching Modulate LHCII Dynamics 6.1. LHCII clustering versus mobility 6.2. NPQ control by LHCII antenna hydrophobicity 7. Formation of the NPQ Quencher(s): Inner LHCII Complex Dynamics 8. Physiological Implications of the Dynamic Properties of LHCII Acknowledgements 210 2212		177
1. Introduction 190 2. The Structure of LHCII Complex and the Landscapes of the Photosystems 191 3. Evidence for the Fast Dynamics of the Photosynthetic Membrane 195 4. LHCII Composition and Membrane Dynamics 197 5. State Transitions are Affected by PSII Antenna Composition 198 6. Zeaxanthin and Non-Photochemical Quenching Modulate LHCII Dynamics 200 6.1. LHCII clustering versus mobility 201 6.2. NPQ control by LHCII antenna hydrophobicity 203 7. Formation of the NPQ Quencher(s): Inner LHCII Complex Dynamics 207 8. Physiological Implications of the Dynamic Properties of LHCII Acknowledgements 2112	Chapter 9 Adaptive Reorganisation of the Light Harvesting And	tenna 189
 Introduction The Structure of LHCII Complex and the Landscapes of the Photosystems Evidence for the Fast Dynamics of the Photosynthetic Membrane LHCII Composition and Membrane Dynamics State Transitions are Affected by PSII Antenna Composition Zeaxanthin and Non-Photochemical Quenching Modulate LHCII Dynamics LHCII clustering versus mobility NPQ control by LHCII antenna hydrophobicity Formation of the NPQ Quencher(s): Inner LHCII Complex Dynamics Physiological Implications of the Dynamic Properties of LHCII Acknowledgements 	_	
2. The Structure of LHCII Complex and the Landscapes of the Photosystems 3. Evidence for the Fast Dynamics of the Photosynthetic Membrane 195 4. LHCII Composition and Membrane Dynamics 5. State Transitions are Affected by PSII Antenna Composition 6. Zeaxanthin and Non-Photochemical Quenching Modulate LHCII Dynamics 6.1. LHCII clustering versus mobility 6.2. NPQ control by LHCII antenna hydrophobicity 203 7. Formation of the NPQ Quencher(s): Inner LHCII Complex Dynamics of LHCII Acknowledgements 210 212		190
of the Photosystems 3. Evidence for the Fast Dynamics of the Photosynthetic Membrane 4. LHCII Composition and Membrane Dynamics 5. State Transitions are Affected by PSII Antenna Composition 6. Zeaxanthin and Non-Photochemical Quenching Modulate LHCII Dynamics 6.1. LHCII clustering versus mobility 6.2. NPQ control by LHCII antenna hydrophobicity 7. Formation of the NPQ Quencher(s): Inner LHCII Complex Dynamics 8. Physiological Implications of the Dynamic Properties of LHCII Acknowledgements 197 200 201 202 203 210 211 211	1. Introduction	
3. Evidence for the Fast Dynamics of the Photosynthetic Membrane 4. LHCII Composition and Membrane Dynamics 5. State Transitions are Affected by PSII Antenna Composition 6. Zeaxanthin and Non-Photochemical Quenching Modulate LHCII Dynamics 6.1. LHCII clustering versus mobility 6.2. NPQ control by LHCII antenna hydrophobicity 203 7. Formation of the NPQ Quencher(s): Inner LHCII Complex Dynamics 8. Physiological Implications of the Dynamic Properties of LHCII Acknowledgements 210 212		191
4. LHCII Composition and Membrane Dynamics 5. State Transitions are Affected by PSII Antenna Composition 6. Zeaxanthin and Non-Photochemical Quenching Modulate LHCII Dynamics 6.1. LHCII clustering versus mobility 6.2. NPQ control by LHCII antenna hydrophobicity 203 7. Formation of the NPQ Quencher(s): Inner LHCII Complex Dynamics 8. Physiological Implications of the Dynamic Properties of LHCII Acknowledgements 210 212	of the Photosystems	195
5. State Transitions are Affected by PSII Antenna Composition 6. Zeaxanthin and Non-Photochemical Quenching Modulate LHCII Dynamics 6.1. LHCII clustering versus mobility 6.2. NPQ control by LHCII antenna hydrophobicity 203 7. Formation of the NPQ Quencher(s): Inner LHCII Complex Dynamics 8. Physiological Implications of the Dynamic Properties of LHCII Acknowledgements 210 212	3. Evidence for the Past Dynamics of the Pasters	197
6. Zeaxanthin and Non-Photochemical Quenching Modulate LHCII Dynamics 200 6.1. LHCII clustering versus mobility 201 6.2. NPQ control by LHCII antenna hydrophobicity 203 7. Formation of the NPQ Quencher(s): Inner LHCII Complex Dynamics 207 8. Physiological Implications of the Dynamic Properties of LHCII 210 Acknowledgements 212	4. LHCII Compositions are Affected by PSII Antenna Composition	198
Dynamics 6.1. LHCII clustering versus mobility 201 6.2. NPQ control by LHCII antenna hydrophobicity 203 7. Formation of the NPQ Quencher(s): Inner LHCII Complex Dynamics 207 8. Physiological Implications of the Dynamic Properties of LHCII Acknowledgements 210 212	5. State Transitions are Americal Ouenching Modulate LHCII	
6.1. LHCII clustering <i>versus</i> mobility 6.2. NPQ control by LHCII antenna hydrophobicity 203 7. Formation of the NPQ Quencher(s): Inner LHCII Complex Dynamics 8. Physiological Implications of the Dynamic Properties of LHCII 210 Acknowledgements 211		200
6.2. NPQ control by LHCII antenna hydrophobicity 7. Formation of the NPQ Quencher(s): Inner LHCII Complex Dynamics 8. Physiological Implications of the Dynamic Properties of LHCII Acknowledgements 203 207 210		201
7. Formation of the NPQ Quencher(s): Inner LHCII Complex Dynamics 8. Physiological Implications of the Dynamic Properties of LHCII Acknowledgements 210 212	6.2. NPO control by LHCII antenna hydrophobicity	203
8. Physiological Implications of the Dynamic Properties of LHCII Acknowledgements 210 212	7 Formation of the NPO Quencher(s): Inner LHCII Complex Dynar	mics 207
of LHCII Acknowledgements 212 212	Physiological Implications of the Dynamic Properties	
Acknowledgements 212		210
.1.2		212
		212

Chapter 10 Thylakoid Membrane Dynamics in Higher Plants	221
Haniyeh Koochak, Meng Li, Helmut Kirchhoff	
	221
1. Introduction	223
2. Supramolecular Dynamics	223
2.1. Protein order and disorder in thylakoid membranes	
2.1.1. Significance of mesoscopic dynamics for energy	223
transformation and its regulation 2.1.2. Types of semi-crystalline protein arrays in grana thylakoids	224
2.1.2. Types of semi-crystatine protein arrays in grant and	
2.2. Potential advantages and disadvantages of	225
semi-crystalline protein arrays	226
2.2.1. PSII repair	227
2.2.2. Diffusion in the lipid matrix	228
2.3. Factors controlling mesoscopic protein arrangements	228
2.3.1. Lipids and fatty acids	229
2.3.2. Protein phosphorylation	230
2.4. The elusive mesoscopic level	230
3. Thylakoid Membrane Dynamics	230
3.1. Types of thylakoid lumen swelling and shrinkage	232
3.2. Factors controlling thylakoid membrane dynamics	232
3.2.1. Ion transporters	233
3.2.2. Protein kinases and phosphatases	233
3.2.3. Membrane curvature proteins	234
3.3. Controversies of observed thylakoid dynamics	235
Acknowledgements	235
References	200
Chapter 11 Oxygenic Photosynthesis — Light Reactions	
within the Frame of Thylakoid Architecture	
and Evolution	243
Sari Järvi, Marjaana Rantala and Eva-Mari Aro	
	244
1. Introduction	
 Thylakoid Membrane Heterogeneity — From Cyanobacteria 	244
to Higher Plants	246
3. Key Regulatory Mechanisms of Thylakoid Electron Transfer Reactions	246
3.1. No clear model organism for regulation of light reactions	2,0
3.2. Evolution of key regulatory mechanisms of thylakoid	247
electron transfer reactions	2411
4. Factors Regulating the Thylakoid Architecture	250
in Oxygenic Photosynthetic Organisms	0.50

Contents	AV
5. Revealing the Dynamics of Thylakoid Architecture	
in Higher Plant Chloroplasts	251
5.1. Methods to study thylakoid heterogeneity —	251
Dark acclimated plants	251
5.2. Thylakoid fractionation from light-acclimated plants	
demonstrates light-dependent, reduced stringency of	256
lateral heterogeneity 5.3. Significance of thylakoid plasticity for photosynthetic	200
light reactions and beyond	258
Acknowledgments	259
References	259
Chapter 12 Estimation of the Cyclic Electron Flux around Photosystem I in Leaf Discs	265
Jiancun Kou, Duncan Fitzpatrick, Da-Yong Fan,	
Shunichi Takahashi, Riichi Oguchi and Wah Soon Chow	266
1. Introduction	267
2. Partitioning of Absorbed Light Between the Two Photosystems	268
3. Cyclic Electron Flux in Spinach Leaves	269
4. Cyclic Electron Flux in Arabidopsis Leaves	269
4.1. CEF in wild type Arabidopsis 4.2. CEF in the pgr5 mutant of Arabidopsis	270
4.2. CEF in the pgr3 mutant of Arabidopsis 4.3. CEF in the ndh mutant of Arabidopsis	270
4.4. The antimycin A-sensitive component of <i>ETR1</i> in <i>Arabidopsis</i>	270
5. Concluding Remarks	272
Acknowledgements	273
References	273
Chapter 13 The Contribution of Electron Transfer after	
Chapter 13 The Contribution of Electron Transfer after Photosystem I to Balancing Photosynthesis	277
Guy Hanke and Renate Scheibe	
1. Introduction	278
2. The Hierarchy of Electron Donation	281
3. Diversity Among Electron Carriers	285
4. Regulation of Sink Demand Beyond the First Acceptor	288
5. Flexible Adjustment of Target-Enzyme Activity According	200
to Metabolic Demand	290
6. Signaling upon Redox-Imbalances for Long-Term Adaptation at the	291
Transcriptional Level	292
References	

Chapter 14 Cyclic Electron Flow in Cyanobacteria and Eukaryotic Algae	305
A. W. D. Larkum, M. Szabo, D. Fitzpatrick and J. A. Raven	
	306
 Introduction In Vivo Evidence of Cyclic Photophosphorylation in Algae 	306
a. 1. Occamiovy	306
2.2. Energetics of the assimilation of exogenous glucose and	310
2. Detailed Machanism of Cyclic Electron Transport and	315
ATP Formation in Oxygenic Photosynthetic Organisms	315
0.1 Orrowalovi	
3.1. Overview 3.2. Non-cyclic (= linear) electron flow, cyclic electron flow,	316
the Q cycle and ATP generation	
3.3. Early evolution of NAD dehydrogenases — Bacteria,	317
cyanobacteria, plastids and mitochondria.	317
3.4. Mechanisms for CEF in Cyanobacteria.	
3.5. Detailed mechanism and inhibitors	319
of the NDH system 3.6. Towards a better understanding of cyanobacterial CEF	320
4. Cyclic Electron Transport Complexes of Chlamydomonas and	200
Other Green Algae	322 322
4.1 Introduction	323
10 DCD5/DCDI 1 complexes in thylakoids	323 324
4.2. Deductages of thylakoid membranes and then role in CEA	326
5 Evidence for Cyclic Electron Transport in Eukaryotte Mgas	326
5.1 Dimonhyta (1)motlagellata)	326
5.1. Symbiodinium sp., the coral endosymbiont algae	327
5.2. Haptophyta	327
5.2.1. Prymnesiophyceae	327
5.3. Ochrophyta	327
5.3.1. Bacillariophyceae	328
5.3.2. Eustigmatophyceae	328
5.3.3. Phaeophyceae	328
5.4. Rhodophyta	328
5.4.1. Bangiophyceae	328
5.4.2. Floridiophyceae	

Contents	xvii
6. The Role of CEF in Eukaryotic Algae in a Range of Habitats	329
6.1. Desiccation	329
6.2. Variations in salinity	329
6.3. Low temperature	329
6.4. High temperature	330
6.5. High light	330
6.6. Nitrogen deficiency	330
6.7. Iron deficiency	330
6.8. Summary and Conclusions	331
Acknowledgements	332
References	332
Index	345

Chapter 2

Free, Stalled, and Controlled Rotation Single Molecule Experiments on F₁-ATPase and their Relationships

Sándor Volkán-Kacsó* and Rudolph A. Marcus†

Noyes Laboratory of Chemical Physics,
1200 E. California Blvd., Pasadena, CA 91125, USA

*svk@caltech.edu,

†ram@caltech.edu

We show how an elastic group transfer theory can be used to interpret and treat free, stalling, and controlled rotation single molecule experiments on F₁-ATPase. It is shown how predictions can be made and tested within this class of experiments using our recent theoretical treatment of rotor angle dependent rate constants for this biological motor. The theory is also used to suggest an additional type of analysis of single molecule trajectories involving dwell angles.

1. Introduction

It is a pleasure to participate in this volume honoring our colleagues John Walker and Les Dutton. This chapter includes some of the results that we presented at their joint 75th birthday symposium. It touches on both their works, since it is on studies of F_1 -ATPase, single molecule studies that rely heavily on John's structural discoveries, and it uses the functional form of a rate equation that expresses the activation free energy of each reaction step in terms of the standard free energy and "reorganization energy" λ for that step. The equation was originally derived for electron transfers, a field in which Les has made many contributions, some of them using this equation. This equation has now been adapted, as in earlier work

[e.g. Marcus, 1968], to treat transfer reactions [Sutin, 1968; Murdoch, 1983; Lewis and Hu, 1984] that are unrelated to electron transfers.

The chapter is organized as follows: In Section 2 some of the experimental background in single molecule experiments is summarized, in particular, the free rotation, stalling and controlled rotation experiments. In Section 3 the functional form of the free energy of activation *versus* standard free energy of reaction for the various processes is described and used to obtain an equation for the various rotor angle dependent rate constants. Experimental results are described in Section 4. A theory of the free rotation experiments used by us [Volkán-Kacsó and Marcus, 2015] is described in Section 4, leading to Eq. (13), that was used to extract a key quantity (ΔG_0^0) that is used in predicting angle dependent rate constants in other experiments. The derivation is based on fluctuations from a "dwell" angle and angle dependent rate constants.

In Section 4.3 the dwell angles and substeps are discussed. For concreteness and self consistency we use in this article the dwell angles estimated in single molecule experiments, but since the equations are expressed in terms of the symbols θ_i and θ_f other values can be used instead. It is shown in Section 4.3 how an approximate difference in dwell angles for two successive reaction steps can be predicted from kinetic studies. It is applied to the ATP binding step and to the hydrolysis step. The results illustrate how incomplete or sparse data, in this case for the hydrolysis step, can be used and is particularly helpful when the existing kinetic data are very sparse, as they are for the hydrolysis step.

The biological function of the F_0F_1 -ATP synthase is to regenerate, from ADP and Pi, "spent" ATP molecules used as a "fuel" in a multitude of cellular processes. [Boyer, 1993] ATP synthesis being energetically uphill, it is achieved by coupling a unidirectional mechanical rotation of a central γ shaft in the F_0 ring, prompted by a local proton transfer between offset ion channels in the F_0 (E.g., [Junge and Nelson, 2015]), and the chemistry in the F_1 ring. Single-molecule studies have been thus far focused on the study of the water-soluble F_1 -ATPase, [e.g., Noji et al., 1997; Yasuda et al., 2001; Adachi et al., 2012; Sielaff et al., 2008; Spetzler et al., 2009; Watanabe et al., 2010] a complex formed by the F_1 ring and the γ shaft, which functions in a reverse direction and converts the free energy of the inverse process, ATP hydrolysis, to unidirectional rotation in the opposite direction.

Single molecule techniques have thus been providing quantitative data on the dynamics of the component F_1 of F_0F_1 -ATP synthase, complementing ensemble biochemical and structural experiments [Braig *et al.*, 2000; Boyer, 1993; Senior, 2007; Weber, 2010]. In treating research data, typically in the hydrolysis direction of the F_1 -ATPase motor, the goal is that the mechanism for the enzyme ATP synthase can be elucidated, assuming reversibility in the chemo-mechanical rotation Scheme [Adachi *et al.*, 2007, 2012].

In the present article we analyze three types of single molecule studies: stalling, controlled rotation and free rotation experiments using a chemo-mechanical theory. Controlled rotation data were predicted using the stalling data [Volkan-Kacso and Marcus, 2016]. We derive in Section 3.1 an equation, Eq. 2, that we assumed previously in treating the free rotation experiments. This equation is key to relating the properties of the latter system to the quasistatic rate constants extracted from the stalling and controlled rotation experiments.

We review in Section 3 a chemical-mechanical theory [Volkán-Kacsó and Marcus, 2015] that we formulated to treat several types of single molecule experiments on a biomolecular motor [Adachi et al., 2007, 2012]. The theory is adapted from a theory of electron and other transfers in solution [Marcus, 1968; Marcus and Sutin, 1985; Marcus, 1993] and in addition contains the torsional elasticity effect [Sielaff et al., 2008] in the motor in the various physical and chemical processes, such as ATP binding and ATP hydrolysis.

2. Description of Three Single-Molecule Experiments

2.1. Free rotation experiments: Stepping rotation and concerted kinetics

By attaching the F_1 "stator" ring subunit to a microscope slide the rotation of the "rotor" shaft has been monitored by dark field and fluorescent single molecule microscopy. In one version of this experiment a microfilament was attached to the rotor which rotates under heavy viscous load due to friction in the solution [Noji *et al.*, 1997]. When the viscous drag was reduced by replacing the probe with a submicronsized bead, a counter-clockwise stepping rotation (when viewed from the F_0 side) with dwell angles 120° apart was resolved [Adaci *et al.*, 2000]. Later, substeps of 40° and 80° were resolved using a lower ATP concentration [Yasuda *et al.*, 2001].

A chemo-mechanical scheme shown in Figure 1 has been established by a series of single-molecule experiments, in which ATP binding and ADP release (from a different β subunit) are concerted events (80° substep) and ATP hydrolysis and Pi release (again, from a different β subunit) occur during a 40° substep [Nishizaka et al., 2004; Adachi et al., 2007; Senior, 2007; Watanabe et al., 2010]. In the scheme, when following the events in the same subunit, ATP binding occurs during the 80° step following a binding dwell set to 0° [Yasuda et al., 2001]. The ATP does not undergo hydrolysis until much later in the rotation, during the 200° to 240° step, a 40° step. ADP release follows during the subsequent 80° step, from 240° to 320°. Finally, Pi release occurs during the last 40° step, from 320° to 360°.

The timescale of rotation of the γ subunit the biochemically active ATP synthase is comparable to that occurring in the free rotation experiments (ms).

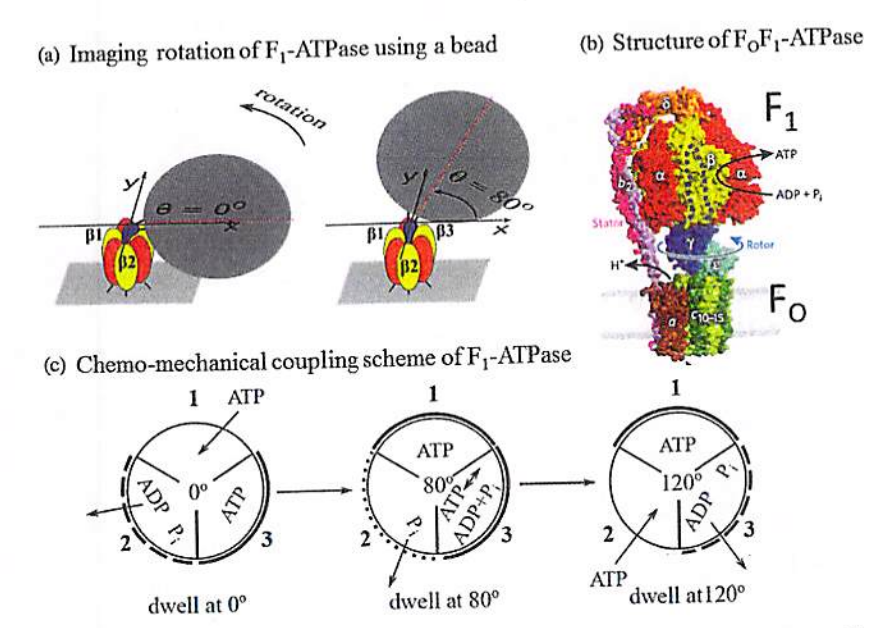


Figure 1. (a) Imaging rotation of F_1 -ATPase with rotor fixed to the microscope slide and imaging bead attached to the rotor. The example shows a step of 80°. (b) Structure of the complete membrane embedded F_1F_0 -ATPase, seen upside-down relative to the F_1 -ATPase in a, reproduced from Weber [2010] with journal permission. (c) Scheme of coupled processes in F_1 -ATPase during free rotation. The dwell angle increases in the counter clockwise direction. The species occupying the pockets of ring β subunits 1, 2 and 3.

We note that a high-speed rotation assay using gold nanorods as probes attached to the shaft [Spetzler et al., 2009] permitted the study of the angular velocity of the rotor during the transition between dwells (timescales of μ s). In this article we focus instead on free rotation experiments (ms) that display the stepping kinetics and yield trajectories from which the angle-dependent rate constant data were extracted from the dwell times. More will undoubtedly be learned from the short timescale fast rotation on the physiological timescale.

2.2. Stalling experiments

In these experiments the imaging beads were replaced by double beads possessing a permanent magnetic dipole moment [Adachi *et al.*, 2012]. When these micromagnets were attached to the rotor (Figure 2a) and an external magnetic field was applied, the rotor aligned itself to the direction of the controlling external magnetic field. The setup, termed *magnetic tweezers*, can be used to set an arbitrary rotor angle θ .

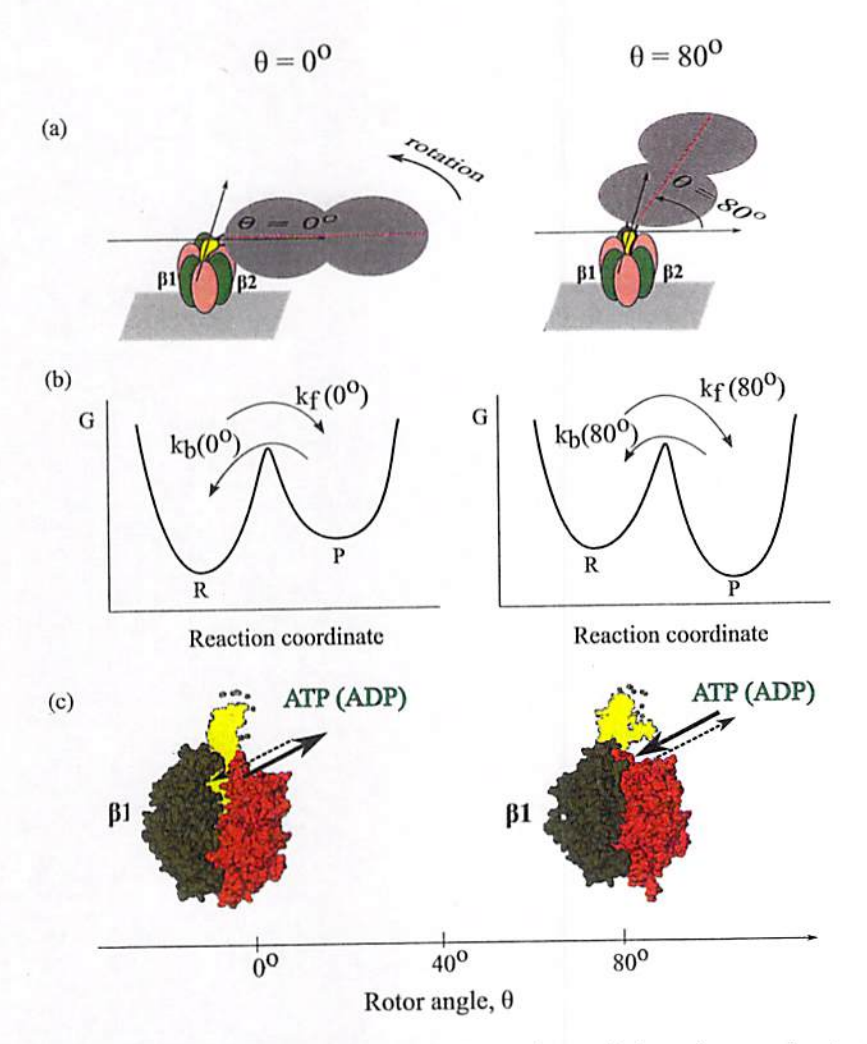


Figure 2. (a) F_1 -ATPase in single molecule imaging and controlled rotation experiments at two rotor angles: 0° and 80° . A double-bead is attached to the γ rotor shaft (in yellow) and rotated against the stator ring (active subunits β_1 - β_3). (b) Free energy profile for nucleotide binding (k_f) and release (k_b) rate constants at the two angles. (c) Open-to-close changes in the nucleotide binding β_1 subunit as a function of rotor angle.

Noji and coworkers have devised an ingenious stalling technique for using the magnetic tweezers to extract rate constant data [Watanabe *et al.*, 2010]. In these stalling experiments, a freely rotating shaft was allowed to reach a dwell angle (*e.g.*, the binding dwell), then the tweezers were immediately activated to set the rotor to an arbitrary angle θ . The rotor was then stalled at θ for a given time, after which it was released and it either moved back to the original dwell or forward to the next dwell.

After repeating these experiments for a series of dwell times, Adachi et al. [2012] interpreted the statistics of forward and back rotations in terms of a two-state model. They assumed that (1) during the stall time, the system can undergo several forward and backward processes, and (2) the rotations (forward or back) upon release depended on the state of the underlying process (e.g., for ATP binding either ATP-bound or empty) at the moment of release. The observed relative number of forward and back events as a function of stall time yielded the forward (k_p) and backward (k_b) rate constants of ATP binding, or other processes. The model of elastic transfer of nucleotides was proposed to explain this rate constants versus θ data in terms of the effect of the elastic response of the rotor structure on the free energy surface (Figure 2b) [Volkán-Kacsó and Marcus, 2015].

2.3. Controlled rotation experiments

By replacing the "wild-type" nucleotides, ATP or ADP, by a modified nucleotide that fluoresces, single-molecule fluorescence microscopy was used to monitor individual binding and release events [Adachi *et al.*, 2007]. In particular, a fluorescent Cy3 moiety was attached to the nucleotides *via* a flexible alkane tether. In the experiments, when the Cy3-nucleotide bound to the F₁-ATPase the Cy3 moiety emitted a fluorescence signal but when it was in the solution the fluorescence was quenched.

Adachi et al. [2012] employed the fluorescence Cy3-nucleotide in conjunction with the rotation microscopy and magnetic tweezers using the micro-bead probes. To do so, the shaft was rotated at a constant rate and the individual binding and release events of fluorescent nucleotides, and so the site occupancy, were directly monitored [Adachi et al., 2012]. By keeping a low ATP concentration, events of occupancy changing between 0 and 1 were determined and analyzed (Figure 2c). Using a grouping criterion of binding and release times, the number of $(0 \rightarrow 1)$ and $(1 \rightarrow 0)$ events state yielded forward and reverse rate constants as a function of rotor angle. The feature that is especially informative is comparing the results of such low occupancy experiments with the physiologically relevant experimental results where the occupancy is 2 or 3.

3. Group Transfer Theory in Stalling and Controlled Rotation Experiments

We give in this section an overview of the group transfer theory first proposed to treat the stalling experiments [Volkán-Kacsó and Marcus, 2015] and then used to predict controlled rotation experiment data [Volkán-Kacsó and Marcus, 2016], and later including composite events to extract hydrolysis and synthesis data from the trajectories [Volkán-Kacsó and Marcus, 2017]. Then, using the theoretical

framework, the average rate constants extracted from dwell distributions in the free rotation experiments were then calculated.

3.1. Angle dependent rate constants and free energies

In a transition-state picture, the activation free energy barrier ΔG^* for a reaction determines the rate constant of the process. The rate constant k is given by

$$k = A \exp(-\Delta G^*/kT) \tag{1}$$

where A depends on the reaction order and the details of the transition state of the process. For a bimolecular process the A can be expressed in terms of a collision theory [Volkán-Kacsó and Marcus, 2015] in treating ATP binding that involves a weak binding site of an empty β subunit. The pre-exponential term A is a collision frequency Z, and a term related to an ATP binding outside of the β subunit. For the binding and release of ATP there are extensive single molecule data obtained by different methods [Yasuda $et\ al.$, 2001; Spetzler $et\ al.$, 2009; Watanabe $et\ al.$, 2010; Braig $et\ al.$, 2000; Watanabe $et\ al.$, 2012, Adachi $et\ al.$, 2012]. In the ATP binding an ATP first forms a collision complex with the F_1 -ATPase, followed by an ATP binding in an 80° step in the overall hydrolysis direction [Oster and Wang, 2000].

To treat the free energy barrier in Eq. (1), we note that the equations of the "weak-overlap" theory of electron transfer reactions were adapted to treat "strong overlap" reactions, such as the transfer of an atom in a reaction [Marcus, 1968; Marcus and Sutin, 1985; Marcus, 1993]. We have applied this idea to treat the transfer of an even larger species, such as a nucleotide, ATP or ADP, during binding to the F_1 -ATPase, while the rotor angle θ is fixed, e.g., as in the stalling experiments. Taking into account a work term W^r for attaching the ATP from solution to the exterior of the F_1 -ATPase (a weak binding site), to the binding pocket (strong binding site) the well-known quadratic equation is written as a function of the rotor angle θ .

$$\Delta G^*(\theta) = W^r + [\lambda + \Delta G^0(\theta)]^2 / 4\lambda. \tag{2}$$

In Eq. (2) ΔG^0 denotes the standard free energy reaction of the transfer process, a function of θ , and λ denotes the "reorganization energy" for the reaction. The quadratic formalism has been tested experimentally in its adaptation to strong overlap processes [Sutin, 1968; Lewis and Hu, 1984] and theoretically [Murdoch, 1983]. A related approach leading to a related equation is based on a bond energy-bond order model (BEBO) [Marcus, 1968 and reference cited therein] in which the sum of the bond orders of the reactant and product state bonds is assumed constant during the reaction. It served to explain why the quadratic equation given in Eq. (2) derived initially for weak overlap electron transfer reactions, can be

$$\begin{array}{ccc}
 & \Delta G^{0}(\theta) \\
G_{r}^{0}(\theta) & \rightarrow & G_{p}^{0}(\theta) \\
w^{r} \uparrow & & \downarrow -w^{p} \\
G_{r}^{0}(\theta_{i}) & \rightarrow & G_{p}^{0}(\theta_{f}) \\
 & \Delta G_{0}^{0}
\end{array}$$

Scheme 1.

applied to other transfer reactions. In the BEBO model the activation energy of the transfer is roughly 10% of the total bond energy. It is easier to break a chemical bond if at the same time a new chemical bond is also forming, in this case the process is 10 times easier in terms of energetics. This cooperation is assumed when applying Eq. (2) to the physical processes of binding a nucleotide and release, which involve the breaking and forming of bonds such as hydrogen bonds and "hydrophobic" bonds.

To calculate the θ dependence of the standard free energy of reaction $\Delta G^0(\theta)$ a thermodynamic cycle (Scheme 1) was used [Volkán-Kacsó and Marcus, 2015]. The energy balance around the cycle provides a relationship between the free energies of a ligand binding in free rotation, ΔG_0^0 , and the binding free energy $\Delta G^0(\theta)$ at a constant rotor angle θ .

In Scheme 1, $\Delta G_r^0(\theta)$ and $\Delta G_p^0(\theta)$ are the free energies of the system in the reactant and product states when the rotor is at an angle θ , while $\Delta G_r^0(\theta_i)$ and $\Delta G_p^0(\theta_f)$ are the reactant and product free energies in the relaxed system at dwell angles θ_i and θ_f , respectively. We assume an elastic coupling first suggested by Junge and coworkers [Panke et al., 2001; Sielaff et al., 2008] between the rotor angle and the stator subunit conformation [Volkán-Kacsó and Marcus, 2015] involved in each of these steps. Accordingly, the system, while in the reactant state, can be rotated from a dwell angle θ_i to an arbitrary angle θ by elastically distorting the structure, by doing a work $w_r(\theta)$ provided externally by the external magnetic field of the magnetic tweezers. To achieve a rotation from θ_i to θ , parts of the structure (mainly the rotor and to some extent the lever arm of the β subunit) undergo an elastic twisting deformation of stiffness κ .

Analogously, the F_1 -ATPase in the product state, can be rotated from an angle θ to the relaxed state at θ_f by doing a work $w_p(\theta)$, a work done by the system. To achieve this rotation an elastic twisting deformation of stiffness κ must occur. The elastic work terms then are

$$w' = \frac{\kappa}{2} (\theta - \theta_i)^2$$
 and $w^p = \frac{\kappa}{2} (\theta - \theta_f)^2$. (3)

The energy balance in Scheme 1 requires that

$$\Delta G^{0}(\theta) = \Delta G_{0}^{0} + w^{p}(\theta) - w^{r}(\theta) = \Delta G_{0}^{0} - \kappa (\theta_{f} - \theta_{i})(\theta - \theta_{c}), \tag{4}$$

where the notation $\theta_c = (\theta_f + \theta_i)/2$ was applied and ΔG_0^0 is the free energy change corresponding to the difference between the free energy minima in the final dwell state *versus* that in the initial dwell state. Using Eqs. (1)–(5) we have shown [Volkán-Kacsó and Marcus (2017)] that the theory provides a symmetric expression for the rate constant *versus* rotor angle dependence,

$$kT \ln k_f(\theta) = kTk_f(\theta_c) + (1/2 + \Delta G_0^0/2\lambda) \Delta \theta_r - (\Delta \theta_r)^2/4\lambda,$$

$$kT \ln k_b(\theta) = kTk_b(\theta_c) + (-1/2 + \Delta G_0^0/2\lambda) \Delta \theta_r - (\Delta \theta_r)^2/4\lambda,$$
(5)

where $\Delta\theta_r = \kappa(\theta_f - \theta_i)(\theta - \theta_c)$ and $\theta_c = (\theta_i + \theta_f)/2$, as defined in Volkán-Kacsó and Marcus [2015]. The quadratic term is small in the case of the ATP binding step (less than 8% contribution). We note that for the equilibrium constant this dependence is predicted to be exponential,

$$kT \ln K(\theta) = kT \ln K(\theta_c) - \kappa \left(\theta_f - \theta_i\right) (\theta - \theta_c). \tag{6}$$

3.2. Application to ATP binding in the overlapping θ -range

The stalling and controlled rotation experiments are complementary in several respects. Both experiments provide the θ -dependent rate constants and equilibrium constants for the steps in the overall process. There is a region of angles θ roughly -45° to $+45^{\circ}$ where the controlled rotation and stalling data overlap. Important differences are that in the former a fluorescent species, Cy3-ATP and Cy3-ADP, is used instead of ATP and ADP. Further, the nucleotide concentration in the controlled rotation experiments is kept low such that the occupancy is at most 1, while in the stalling experiments the system has the physiologically relevant occupancy 2 to 3 by nucleotides. Due to the finite time resolution of the single molecule fluorescence signal, in the controlled rotation experiments, there are certain missed events when the rate of nucleotide release is very fast. These missed events were calculated using the theory embodied in the previous equations [Volkán-Kacsó and Marcus, 2016].

Turning now to the quantitative analysis of the rate constant *versus* rotor angle data in these experiments, we first note that the $\ln K(\theta)$ seen in Eq. (7) to be linear in θ , in agreement with the experimental data [Volkán-Kacsó and Marcus, 2015]. With data from other ensemble [Boyer, 1993; Weber and Senior, 1997] and single molecule [Yasuda *et al.*, 2001, Adachi *et al.*, 2012; Spetzler *et al.*, 2009] experiments Eqs. (5)–(6) were used to predict [Volkán-Kacsó and Marcus, 2015] for the stalling experiments on ATP binding the Bronsted slope $\alpha = \partial \ln k_f / \partial \ln K$ of 0.47,

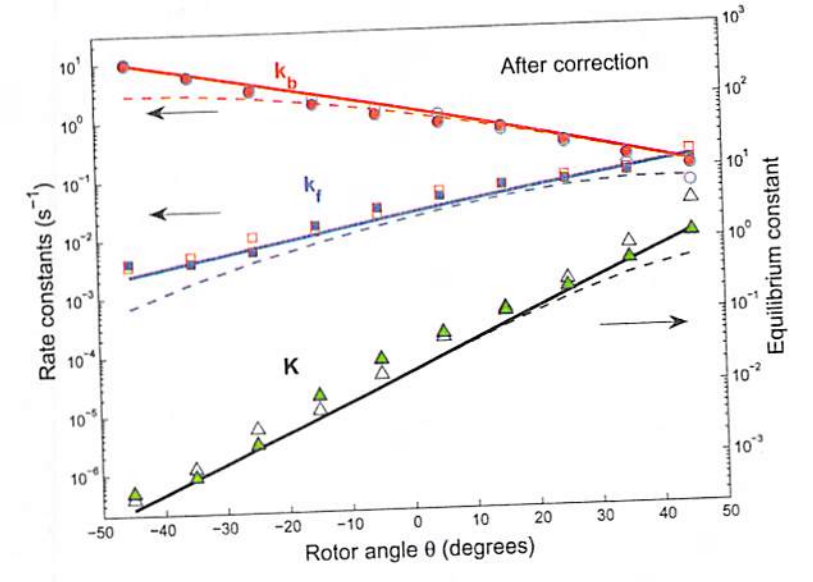


Figure 3. Corrected binding and release rate and equilibrium rate constants *versus* θ angle for Cy3-ATP in the presence (solid squares, circles and triangles) and absence of Pi (open symbols) in solution adapted from Volkán-Kacsó and Marcus [2016]. The experimental data of Adachi *et al.* [2012] corrected for missed events (and an error due to replacing the time spent in the empty state by total time of a trajectory) are compared with their theoretical counterparts (solid lines). Dashed lines show the data without corrections.

which compares with the value of 0.48 in the stalling experiment for the rate of ATP binding and release over the θ range studied. For the ATP binding rate k_f the predicted slope of the $\ln k_f(\theta)$ versus θ was found to be in reasonable agreement (~within 10%) with experiment [Volkán-Kacsó and Marcus, 2015]. For the spring constant κ of the rotor that appears in Eq. (3) the value of $\kappa = 16$ pN nm rad-2 obtained from the stalling experiments was used.

The stalling data, supplemented by ensemble data, was used to predict, using Eq. (5), the rate constants in the controlled rotation experiments with no adjustable parameters. The comparison is given in Figure 3, in the θ -range of overlap. Good agreement was found between these experiments and our calculations, seen there, where the points (symbols) are experimental and the solid curves theoretical data.

3.3. Turnover, near symmetry and long binding events in the controlled rotation experiments

To explain a turnover in binding seen in controlled rotation data seen in Figure 4, it was suggested [Volkán-Kacsó and Marcus, 2016] that a slow diffusion process occurs after the binding to the outside of the enzyme: the diffusion of ATP in a channel at the interface of an α and β subunit, is slowed by the partially closed subunit.

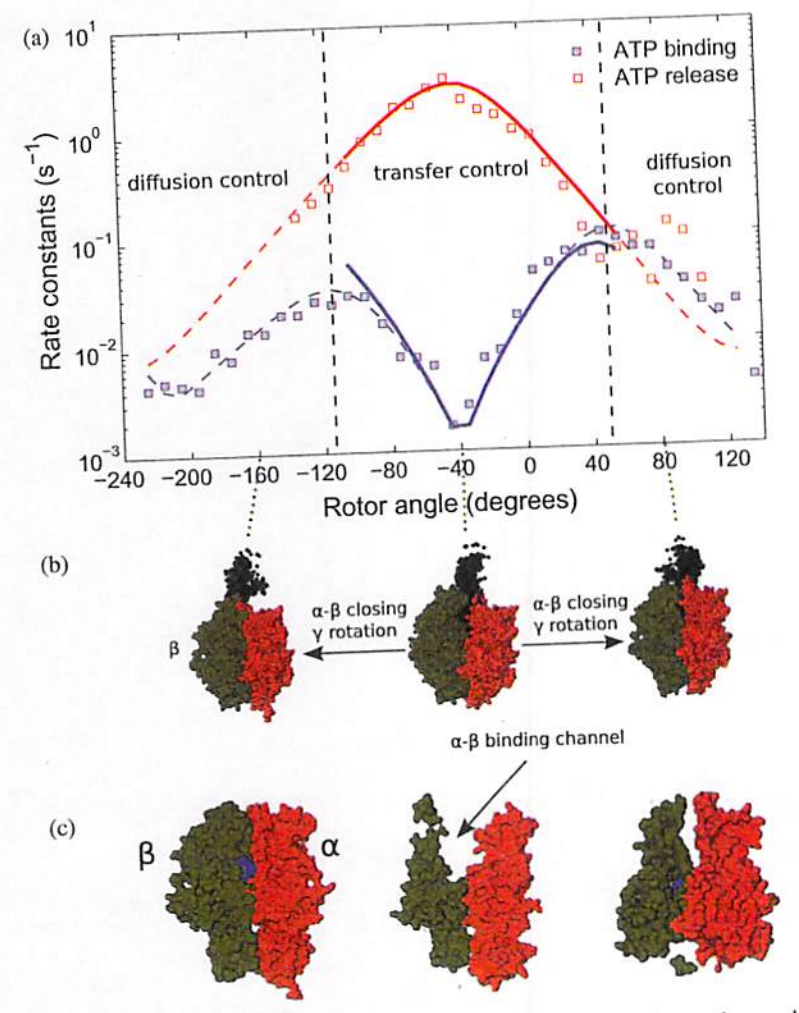


Figure 4. (a) Reported binding and release rate constants *versus* controlled rotation angle for fluorescent ATP in the presence of Pi in solution. The reported uncorrected experimental data (squares) are compared with theoretical counterparts (solid lines) by calculating missed events and also correcting for an error due to replacing the time in the empty state T_0 by the total time T. Dashed lines show a fit to the experimental data. (b) F_1 -ATPase structure at three different rotor angles with β subunits in green, α subunits in red and the γ subunit in black. (c) Cutaway of the three structures revealing the binding channel at the α - β interface and its narrowing as the rotor angle is changed.

Structurally, the turnover indicates that the closing of the binding channel continues as the angle is rotated beyond 80° . The turnover is consistent with structural data showing a continuum of open-to-close states between -40° and 140° . A closure of the binding channel (Figure 4c) as the rotor is moved beyond 80° (Figure 4b) retards the diffusion process and it becomes the bottleneck during binding. In a diffusion-reaction scheme [Marcus, 1960; Noyes, 1961], the transfer reaction is the bottleneck in the θ -region from -120° to $+45^{\circ}$.

In Figure 4c the β subunit is the most open at -40° and the most closed presumably at +140° (0° is defined as the binding dwell angle at which the β subunit in question is empty and is about to undergo ATP binding associated with a subsequent 80° substep). The minimum at -40° does not correspond to a specific dwell angle. Diffusion reaction treatments are given in Noyes [1961] and Marcus [1960].

Recently, this theory of elastic group was further extended [Volkán-Kacsó and Marcus, 2017] to treat the experimentally observed lifetime distribution of long binding events in the controlled rotation. Using these distributions the long binding events in the experiments can be calculated and the rate constants for the hydrolysis and synthesis reactions occurring during these events extracted. As discussed in a later section a near symmetry of the data about the angle of –40° and a "turnover" in the binding rate data *versus* rotor angle for angles greater than about 40° was interpreted using diffusion-reaction kinetics.

4. Application of the Theory to Free Rotation

4.1. Rate constant of a free rotation experiment

In this subsection we derive a key equation Eq. (10), used to obtain some of the quantities, including ΔG_0^0 , used [Volkán-Kacsó and Marcus, 2015] to predict the controlled rotation results from the stalling data. In a free rotation experiment we suppose that the system jumps from θ_i to θ_f during some fluctuation from its initial value θ_i . The probability of a fluctuation in θ is proportional to exp $[-C(\theta)/kT]$ where

$$C(\theta) = \kappa (\theta - \theta_i)^2 / 2. \tag{6}$$

At this θ the free energy of activation for binding for an ATP attached to the outside of an ATPase β -subunit is (apart from a W term in Volkán-Kacsó and Marcus [2015] that we include later as part of a factor A). Using Eq. (2) for the forward rate constant $k_f(\theta)$ one finds that

$$k_{f}(\theta) = A \exp(-\Delta G^{*}(\theta) / kT), \tag{7}$$

where A is given in Volkán-Kacsó and Marcus [2015] and $\Delta G^*(\theta)$ is given by Eq. (2). The average value of the forward rate constant in a free rotation is then given by

$$\left\langle k_{f}\right\rangle = \int_{\theta_{L}}^{\theta_{H}} A e^{-\left[\Delta G^{\dagger}(\theta) + C(\theta)\right]/kT} d\theta / \int_{\theta_{L}}^{\theta_{H}} e^{-C(\theta)/kT} d\theta. \tag{8}$$

We note that the effective integration limits enclose a peak angle θ^* of the integrand, so $\theta_L < \theta^* < \theta_H$, and are determined by the steepness of the integrand about its maximum. If one neglects the term quadratic in $\Delta G^{\circ}(\theta)$ in Eq. (4) (valid, in the case of ATP binding, as seen in the closeness of the Bronsted slope α to the value

0.5) experiment one finds from Eqs. (4)–(7) that the minimum value of exponent in the numerator occurs when θ is given by

$$\theta^* - \theta_i \approx (\theta_f - \theta_i)/2. \tag{9}$$

The integrand of the exponent in the numerator of Eq. 8 is peaked at this angle $\theta = \theta^*$. Using the saddle point method to evaluate the integral, in the first approximation we find that

$$\left\langle k_f \right\rangle \approx k_f(\theta^*), \tag{10}$$

a result used in Volkán-Kacsó and Marcus [2015] to obtain the value of the ΔG_0^0 from the experimental data.

The analysis of the reverse process, ATP release, can be performed in an analogous manner. An important difference is that the initial state for the release, the dwell at 80°, is beyond the interval covered in the stalling experiments. Controlled rotation data can be used to predict the step size and dwell angles, by taking into account the effect of the Cy3 moiety attached to the ATP on binding and release in both controlled and free rotation. Using a functional form for the release rate constant $k_b = A \exp(-\Delta G^b(\theta)/k\Gamma)$, where $\Delta G^b(\theta)$ is the barrier for the ATP release step that can be extracted from the controlled rotation data, the analogue of Eq. (8) is

$$\left\langle k_{b}\right\rangle = \int_{\theta_{L}}^{\theta_{H}} A e^{-\left[\Delta G^{b}(\theta) + C(\theta)\right]/kT} d\theta \left/ \int_{\theta_{L}}^{\theta_{H}} e^{-C(\theta)/kT} d\theta \right. \tag{12}$$

According to Eq. (5) and as described for Pi release in Volkán-Kacsó and Marcus [2015], and for nucleotide release in Volkán-Kacsó and Marcus [2016] the $\Delta G^b(\theta)$ is an approximately linear function of the rotor angle. If the saddle point method is used, Eq. (12) yields in first approximation the analogue of Eq. (10),

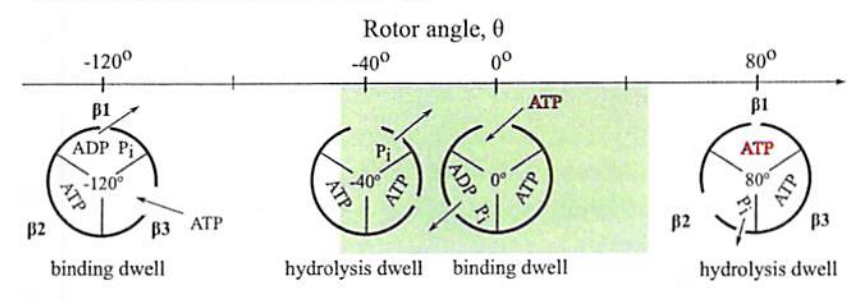
$$\langle k_b \rangle \approx k_b(\theta^*),$$
 (13)

and the maximum will be at $\theta^* = \theta_c = 40^\circ$.

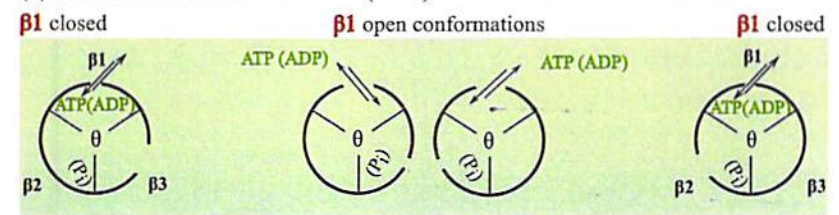
4.2. Relation between controlled and free rotation experiments

The structural changes of opening and closing are consistent with the trends seen in the slopes of the binding and release rate *versus* rotor angle data and with spontaneous stepping rotation. How can the features revealed in stalling and controlled rotation data in Figures 3 and 4 be connected with the rotational kinetics

(a) Stalling experiments and dwell angles



(b) Controlled rotation at low ATP (ADP) concentration



(c) Free stepping rotation and $(\theta_f - \theta_i)$ for nucleotide binding in $\beta 1$

Figure 5. Shaft rotation, nucleotide binding/release activity and conformational changes of a ring subunit in single molecule experiments of stalling (a), controlled rotation (b) and free stepping rotation (c). In (a–c) the system is represented at four different values of the rotor angle, corresponding to dwell angles at -120° , -40° , 0° and 80° . θ is defined relative to subunit 1, *i.e.* $\theta = 0$ for the binding dwell with an empty β subunits.

(Figure 1c) and structural changes? The correspondence between the results of these three experiments, given in the present analysis, based on the theoretical treatment, are summarized in Figure 5.

On the one hand, displacing the rotor to the left or right starting from -40° both accelerate the rate of binding in the controlled rotation experiments. Such displacements of the rotor invariably induce a closing of the β subunit, as seen in the structure in Figure 4c. These effects are consistent with the spontaneous stepping forward rotation induced by binding of ATP in free rotation experiments occurring in a θ -range to the right of -40° (from 0° to 80°).

On the other hand, rotating the rotor towards -40° from the left or from the right both induce an opening of the β subunit which accelerates nucleotide release. This effect, in turn, is consistent with the spontaneous forward rotation induced by the release of ADP in free rotation experiments occurring in a θ -range to the left of -40° (from -120° to -40°).

4.3. Use of the rate constant versus rotor angle data to predict the step size and dwell angles in free rotation

Here we show how the single molecule free rotation kinetics, including step size $(\theta_f - \theta_i)$ and dwell angles θ_i and θ_f of the free system, which cannot be resolved in free rotation assays, can be predicted in the rare case that $\ln K(\theta)$ versus θ is linear over the entire range $(\theta_f - \theta_i)$. It also presents an example of combining different types of sparse data.

The theory has provided simple mathematical relations between the dwell angles, the spring constant and $\ln k_f$, k_b or K versus rotor angle slopes [Volkán-Kacsó and Marcus, 2015; Volkán-Kacsó and Marcus, 2016, 2017]. To predict dwell angles, an independent estimate of the spring constant κ is needed, e.g., from fluctuation experiments.[Sielaff et al., 2008] Using the expression from Eq. (6) for the slope $kT\partial \ln k(\theta)/\partial \theta = K(\theta_f - \theta_i)$ of angle-dependent rate constant, obtained from controlled rotation experiments, the predicted step size in free rotation experiments, $(\theta_f - \theta_i)$ is given by

$$\theta_f - \theta_i = \frac{kT}{\kappa} \frac{\partial \ln K(\theta)}{\partial \theta}.$$
 (14)

In the present application of Eq. (14) for the hydrolysis step the linearity spans an angular range of (150°, 250°) [Watanabe *et al.*, 2012] with θ_i = 200. From these data and Eq. (14) one obtains $\theta_f = \theta_i + 15^\circ = 215^\circ$.

The experimental slope for the equilibrium constant $\partial \ln K(\theta)/\partial \theta = 1.9 \ \text{deg}^{-1}$ and a $\kappa = 16pN \ nm/rad^2$ yield a predicted step size of $\theta_f - \theta_i = 15^\circ$. We note that the stiffness $\kappa = 16pN \ nm/rad^2$ corresponds to the ATP binding step, and we use this value in the present analysis to approximate the κ for the hydrolysis step. Different steps likely have somewhat different κ values, e.g. in Volkán-Kacsó and Marcus [2016] we found for ADP binding a $\kappa = 12pN \ nm/rad^2$ which is smaller than the $\kappa = 16pN \ nm/rad^2$ of ATP binding.

A separate hydrolysis and a Pi release step was not directly resolved in single molecule trajectories, but a difference of about 10° in the stepping size in the $90^{\circ}/30^{\circ}$ and $80^{\circ}/40^{\circ}$ stepping ratio seen in different experiments lead Adachi *et al.* [2007] to speculate that this 10° difference is due to the hydrolysis step. The present calculated value of $\theta_f - \theta_i = 15^{\circ}$ is in reasonable agreement with this assertion, considering the sparsity of the data of Adachi *et al.* [2012]. These data also suggest a Bronsted slope close to unity for the hydrolysis step which we speculate could indicate the presence of two or more substeps during hydrolysis [Shweins and Warshel, 1996]. We note that Eq. (14) does not apply for binding since $\ln K(\theta)$ versus θ is not linear over the whole range of (θ_i, θ_f) for binding (*e.g.*, as seen in the lack of the linearity over the *complete* range in Figure 4a for binding).

In a crystallographic method of studying the kinetic states (dwells) in active rotation Walker and coworkers prepared stable states by using substitutions in the binding species [Bason *et al.*, 2015]. By resolving such the X-ray crystallography structures of mammalian (human and bovine) F_i -ATPase, three stable states were found about 65°, 25° and 30° apart and it was suggested that these states correspond to dwell angles that define the stepping spontaneous rotation of the F_i -ATPase. The 65°, 25° and 30° division is somewhat similar to the 80°, 10° and 30° division proposed from single molecule experiments by Kinosita and coworkers for the thermophilic bacillus F_i -ATPase [Adachi *et al.*, 2007].

5. Concluding Remarks

In the present chapter, we have illustrated how an elastic group transfer theory can be used to treat three types of single molecule experiments: stalling, controlled rotation and free rotation experiments. To do so, we first reviewed the relations for the rate constants of substeps such as ATP binding or ADP release provided using the theory to treat and predict the stalling and controlled rotation data in previous studies [Volkán-Kacsó and Marcus, 2015, 2016, 2017]. A new feature in the present book chapter is the calculation of average rate constant that can be extracted from the dwell time distributions in the free rotation experiments, Eq. (10), used in an earlier work. We also demonstrated how the difference in dwell angles for two successive reaction steps in the free rotation experiments can be predicted from rate constant *versus* rotor angle data from stalling and/or controlled rotation experiments. These predictions were applied to the ATP binding 80° substep, and the hydrolysis substep, supporting an earlier contention that the latter is a small (10°) step.

Acknowledgements

This work was supported by the Office of the Naval Research, the Army Research Office, and the James W. Glanville Foundation.

Appendix

Evaluation of Eq. (8)

We explore here the approximation for ATP binding in more detail by evaluating the numerator and the denominator. For ATP binding $\theta_i = 0^{\circ}$ and $\theta_f = 80^{\circ}$ and we found using the present Eqs. (9) and (10) [Volkán-Kacsó and Marcus, 2015] that $\Delta G_0^0 = 6 \, kcal \, / \, mol \ll 2 \lambda = 136 \, kcal \, / \, mol$ and $\kappa = 16 \, pN \, nm/rad^2$.

In the numerator in Eq. (10), $\theta^* = \theta_c = 40^\circ$ and Eq. 7 is strictly applicable in the θ range covered by stalling experiments of Adachi $et\,al.$ [2012], roughly $-45^\circ < \theta < 45^\circ$. The integrand at the lower bound of $\theta_L \approx -45^\circ$ is smaller than the maximal value by a factor of $\exp\left(1/8\,\beta\kappa\,c^2 - \alpha\lambda^2\right)/\exp\left(-3/4\,\beta\kappa\,c^2 - \alpha\lambda^2\right)\approx \exp\left(5.3\right)\approx 200$. The angle $\theta^* \approx 40^\circ$ is close to a 45° upper bound, and so an empirical functional form can be used as described in Volkán-Kacsó and Marcus [2017], to extend Eq. (7) beyond the turn-over in controlled rotation experiments. In this case, for an upper bound at $\theta_H \approx 60^\circ$, the integrand is estimated to have decayed roughly by a factor of $\exp\left(1/8\,\beta\kappa\,c^2\right)/\exp\left(-1/8\,\beta\kappa\,c^2\right)\approx \exp\left(2.2\right)\approx 9$. Using the saddle-point approximation that treats the integrand as a Gaussian in a $(-\infty, +\infty)$ interval of θ , we have

$$\int_{\theta_L}^{\theta_H} A e^{-\left[\Delta G^{\star}(\theta) + C(\theta)\right]/kT} d\theta \approx \sqrt{2\pi/\kappa} A e^{-\left[\Delta G^{\star}(\theta^{\star}) + C(\theta^{\star})\right]/kT}. \tag{11}$$

In the denominator of Eq. (8) the Gaussian is centered at $\theta^* = 0^\circ$, the elastic approximation in Eq. (6) has been also found to apply within the range of the stalling experiments [Adachi *et al.*, 2012], although it likely applies beyond it [Panke *et al.*, 2001]. For a $\theta_L \approx -45^\circ$ and $\theta_H \approx -45^\circ$ the integrand has decayed relative to the peak by a factor of about exp $(1.34) \approx 4$ so the Laplace approximation yields $\sqrt{2\pi/\kappa} \exp\left(-C\left(\theta^*\right)/kT\right)$.

References

Adachi, K., Oiwa, K., Nishizaka, T., Furuike, S., Noji, H., Itoh, H., Yoshida, M. and Kinosita, K., Jr. (2007). Coupling of rotation and catalysis in F1-ATPase revealed by single molecule imaging and manipulation, *Cell*, 130, 309–321.

Adachi, K., Oiwa, K., Yoshida, M., Nishizaka, T. and Kinosita, K., Jr. (2012). Controlled rotation of the F1-ATPase reveals differential and continuous binding changes for ATP synthesis, *Nat. Commun.*, 3, 1022.

Adachi, K., Yasuda, R., Noji, H., Itoh, H., Harada, Y.S., Yoshida, M. and Kinosita, K., Jr. (2000). Stepping rotation of F1-ATPase visualized through angle-resolved single-fluorophore imaging, *Proc. Natl. Acad. Sci. USA*, 97, 7243–7247.

Boyer, P.D. (1993). The binding change mechanism for ATP synthase—some probabilities and possibilities, *Biochim. Biophys. Acta*, 1140, 215–250.

Braig, K., Menz, R.I., Montgomery, M.G., Leslie, A.G. and Walker, J.E. (2000). Structure of bovine mitochondrial F1-ATPase inhibited by Mg²⁺ADP and aluminium fluoride, *Structure*, 8, 567–573.

Chidsey, C.E.D. (1991). Free energy and temperature dependence of electron transfer at the metal-electrolyte interface, *Science*, 251, 919–922.

Junge, W. and Nelson, N. (2015). ATP synthase, Annu. Rev. Biochem., 84, 631-657.

Lewis, E.S. and Hu, D.D. (1984). Methyl transfers. 8. The Marcus equation and transfers between aerosulfonates, *J. Am. Chem. Soc.*, 106, 3292–3296.

- Marcus, R.A. (1960). Discussion comment on mixed reaction-diffusion controlled rates, *Discuss. Faraday Soc.*, 29, 129.
- Marcus, R.A. (1968). Theoretical relations among rate constants, barriers, and Brønsted slopes of chemical reactions, *J. Phys. Chem.*, 72, 891–899.
- Marcus, R.A. (1993). Electron transfer reactions in chemistry: theory and experiment, including biographical sketch. In *Les Prix Nobel*, Frangsmyr, T., ed., Nobel Foundation (Almqvist & Wiksell, Stockholm, Sweden), p. 63.
- Marcus, R.A. and Sutin, N. (1985). Electron transfers in chemistry and biology, *Biochim. Biophys. Acta*, 811, 265–322 (and references cited therein).
- Masaike, T., Koyama-Horibe, F., Oiwa, K., Yoshida, M. and Nishizaka, T. (2008). Cooperative three-step motions in catalytic subunits of F1-ATPase correlate with 80 degrees and 40 degrees substep rotations, *Nat. Struct. Mol. Biol.*, 15, 1326–1333.
- Murdoch, J.R. (1983). A simple relationship between empirical theories for predicting barrier heights of electron-transfer, proton-transfer, atom-transfer, and group transfer reactions, J. Am. Chem. Soc., 105, 2159–2164.
- Nishizaka, T., et al. (2004). Chemomechanical coupling in F1-ATPase revealed by simultaneous observation of nucleotide kinetics and rotation, *Nat. Struct. Mol. Biol.*, 11, 142–148.
- Noji, H., Yasuda, R., Yoshida, M. and Kinosita, K., Jr. (1997). Direct observation of the rotation of F1-ATPase. *Nature*, 386, 299.
- Noyes, R.M. (1961). Effects of diffusion rates on chemical kinetics, *Prog. React. Kinet.*, 1, 129–160.
- Oster, G. and Wang, H. (2000). Reverse engineering a protein: the mechanochemistry of ATP synthase, *Biochim. Biophys. Acta*, 1458, 482–510.
- Panke, O., Cherepanov, D.A., Gumbiowski, K., Engelbrecht, S. and Junge, W. (2001). Viscoelastic dynamics of actin filaments coupled to rotary F-ATPase: angular torque profile of the enzyme. *Biophys. J.*, 81, 1220–1233.
- Sakaki, N., Shimo-Kon, R., Adachi, K., Itoh, H., Furuike, S., Muneyuki, E., Yoshida, M. and Kinosita, K., Jr. (2005). One rotary mechanism for F1-ATPase over ATP concentrations from millimolar down to nanomolar, *Biophys. J.*, 88, 2047–2056.
- Schweins, T. and Warshel, A. (1996). Mechanistic analysis of the observed linear free energy relationships in p21^{ras} and related systems, *Biochem.*, 35, 14232–14243.
- Senior, A.E. (2007). ATP synthase: motoring to the finish line, Cell, 130, 220-221.
- Sielaff, H., Rennekamp, H., Engelbrecht, S. and Junge, W. (2008) Functional halt positions of rotary F₀F₁-ATPase correlated with crystal structures, *Biophys. J.*, 95, 4979–4987.
- Spetzler, D., Ishmukhametov, R., Hornung, T., Day, L.J., Martin, J. and Frasch, W.D. (2009). Single molecule measurements of F1-ATPase reveal an interdependence between the power stroke and the dwell duration. *Biochemistry* 48, 7979.
- Sugawa, M., Okazaki, K.-I., Kobayashi, M., Matsui, T., Hummer, G., Masaike, T. and Nishizaka, T. (2016). F1-ATPase conformational cycle from simultaneous singlemolecule FRET and rotation measurements, *Proc. Natl. Acad. Sci. USA*, 113, E2916–E2924.

- Sutin, N. (1966). The kinetics of organic reactions in solution, *Annu. Rev. Phys. Chem.*, 17, 119–172.
- Uchihashi, T., Iino, R., Ando, T. and Noji, H. (2011). High-speed atomic force microscopy reveals rotary catalysis of rotorless F1-ATPase, *Science*, 333, 755–758.
- Volkán-Kacsó, S. and Marcus, R.A. (2015). Theory for rates, equilibrium constants, and Brønsted slopes in F1-ATPase single molecule imaging experiments, *Proc. Natl. Acad. Sci. USA*, 112, 14230–14235.
- Volkán-Kacsó, S. and Marcus, R.A. (2016). Theory of controlled rotation experiments, predictions, tests and comparison with stalling experiments in F1-ATPase, *Proc. Natl. Acad. Sci. USA*, 113, 12029–12034.
- Volkán-Kacsó, S. and Marcus, R.A. (2017). Theory of long binding events in single-molecule-controlled rotation experiments on F1-ATPase, Proc. Natl. Acad. Sci. USA, 114, 7272–7277.
- Walker, J.E. (2013). The ATP synthase: the understood, the uncertain and the unknown, *Biochem. Soc. Trans.*, 41, 1–16.
- Watanabe, R., Iino, R. and Noji, H. (2010). Phosphate release in F1-ATPase catalytic cycle follows ADP release, *Nat. Chem. Biol.*, 6, 814–820.
- Watanabe, R., Okuno, D., Sakakihara, S., Shimabukuro, K., Iino, R., Yoshida, M. and Noji, H. (2012). Mechanical modulation of catalytic power on F1-ATPase, *Nat. Chem. Biol.*, 8, 86.
- Watanabe, R. and Noji, H. (2014). Timing of inorganic phosphate release modulates the catalytic activity of ATP-driven rotary motor protein, *Nat. Commun.*, 5, 3486.
- Weber, J. (2010). Structural biology: toward the ATP synthase mechanism, *Nat. Chem. Biol.*, 6, 794–795.
- Weber, J. and Senior, A.E. (1997). Catalytic mechanism of F1-ATPase. *Biochim. Biophys. Acta*, 1319, 19–58.
- Yasuda, R., Noji, H., Yoshida, M., Kinosita, K., Jr. and Itoh, H. (2001). Resolution of distinct rotational substeps by submillisecond kinetic analysis of F1-ATPase, *Nature*, 410, 898–904.
- Zimmermann, B., Diez, M., Zarrabi, N., Gräber, P. and Börsch, M. (2005). Movements of the ε-subunit during catalysis and activation in single membrane-bound H+-ATP synthase, *EMBO J.*, 24, 2053–2063.